Title

Biomechanical defects and rescue of cardiomyocytes expressing pathologic nuclear lamins

Journal

Cardiovascular Research, 114(6)

ISSN

1015-5007

Authors

Laurini, Erik
Martinelli, Valentina
Lanzicher, Thomas
et al.

Publication Date

2018-05-01

DOI

10.1093/cvr/cvy040

Peer reviewed

ESC European Society of Cardiology

Cardiovascular Research (2018) **114**, 846–857
doi:10.1093/cvr/cvy040

Biomechanical defects and rescue of cardiomyocytes expressing pathologic nuclear lamins

Erik Laurini[1†], Valentina Martinelli[2†], Thomas Lanzicher[1†], Luca Puzzi[1], Daniele Borin[1], Suet Nee Chen[3], Carlin S. Long[3], Patrice Lee[4], Luisa Mestroni[3], Matthew R.G. Taylor[3], Orfeo Sbaizero[1]*, and Sabrina Pricl[1]

[1]Department of Engineering and Architecture, University of Trieste, 34127 Trieste, Italy; [2]International Center for Genetic Engineering and Biotechnology, 34149 Trieste, Italy; [3]Cardiovascular Institute and Adult Medical Genetics, University of Colorado Denver Anschutz Medical Campus, Aurora, CO 80045, USA; and [4]Array BioPharma Inc., Boulder, CO 80301, USA

Received 10 August 2017; revised 6 January 2018; editorial decision 7 February 2018; accepted 7 February 2018; online publish-ahead-of-print 8 February 2018

Time for primary review: 37 days

Aims Given the clinical impact of *LMNA* cardiomyopathies, understanding *lamin* function will fulfill a clinical need and will lead to advancement in the treatment of heart failure. A multidisciplinary approach combining cell biology, atomic force microscopy (AFM), and molecular modeling was used to analyse the biomechanical properties of human lamin A/C gene (*LMNA*) mutations (E161K, D192G, N195K) using an *in vitro* neonatal rat ventricular myocyte model.

Methods and results The severity of biomechanical defects due to the three *LMNA* mutations correlated with the severity of the clinical phenotype. AFM and molecular modeling identified distinctive biomechanical and structural changes, with increasing severity from E161K to N195K and D192G, respectively. Additionally, the biomechanical defects were rescued with a p38 MAPK inhibitor.

Conclusions AFM and molecular modeling were able to quantify distinct biomechanical and structural defects in *LMNA* mutations E161K, D192G, and N195K and correlate the defects with clinical phenotypic severity. Improvements in cellular biomechanical phenotype was demonstrated and may represent a mechanism of action for p38 MAPK inhibition therapy that is now being used in human clinical trials to treat laminopathies.

Keywords Lamin A/C • Cardiomyopathy • Cell physiology • Cardiomyocytes • Molecular modeling • AFM

1. Introduction

Nuclear lamins are filamentous proteins providing structural support and transcriptional regulation of the cell nucleus. A-type lamins form a molecular scaffold under the inner nuclear membrane and are structurally connected with the cytoplasm by binding integral proteins of the nuclear envelope that act as 'linkers of the nucleoskeleton and cytoskeleton' (LINC). The importance of nuclear lamins is illustrated by genetic defects in the lamin A/C gene (*LMNA*) that lead to inherited cardiac and skeletal myopathies[1] such as dilated cardiomyopathy, limb-girdle muscular dystrophy, and Emery-Dreifuss muscular dystrophy. The localization of phenotypes to mechanically active tissues has suggested that *LMNA* mutations could render mechanically active muscle cells more susceptible to biomechanical stress.[2] Here, we report the biomechanical cellular effects of three human cardiomyopathy *LMNA* mutations. The clinical phenotypes associated with these *LMNA* cardiomyopathy mutations include global myocardial dysfunction, heart failure, arrhythmia, and sudden cardiac death. However, little is known about the structure–function relationships of individual mutations at the cellular and protein levels. Nuclear lamins are intermediate filaments based on a structure consisting of the short unstructured N-terminal head domain, a long α-helical central rod domain followed by another largely unstructured C-terminal domain with a single immunoglobulin-like (Ig) domain.[3] The central rod domain (α-helical) is distributed into four regions designated as coils 1A, 1B, 2A, and 2B.[4–6] All three mutations considered in this study are located in the central α-helical rod domain at the distal end of coil 1B. This highly conserved region of the lamin A/C protein is critical for the formation of the α-helical coiled-coil dimer, the basic building block for

* Corresponding author. Tel: +39 040 558 3770; fax: +39 040572044, E-mail: sbaizero@units.it

† The first three authors contributed equally to the study.

the construction of lamin filaments. Mutations in this section likely prejudice the dimerization and formation of higher order filaments of lamin. It has been shown[7] that although at the dimer level coil 1B and 2B showed similar elastic behavior, the 1B is more robust, it has higher elastic modulus and therefore higher load bearing capacity. Based on the aforementioned reasons and being the 1B domain the largest domain it is considered as a hot spot for lamin mutations. In fact, almost 40% of these mutations cluster in the rod domain of which nearly 76% are concentrated in 1B and 2B.[8]

To understand these structure–function relationships we investigated the well-described mutations Glu161Lys (E161K, rs28933093), Asp192Gly (D192G, rs57045855), and Asn195Lys (N195K, rs28933091). The biomechanical effect of these mutations and the possibility of a correlation of mechanical defects with the severity of the cardiomyopathy phenotype have never been investigated. To address this gap, we quantitatively characterized the biomechanical phenotype of these *LMNA* mutations using atomic force microscopy (AFM). Specifically, we used the AFM force-deformation test, also called single-cell force spectroscopy (SCFS), to assess the nuclear Young modulus, the cytoskeletal viscoelastic properties and the work of adhesion. Adhesion in this case is defined as the process of detachment of the cell membrane from the AFM tip.

Additionally, we modeled the stiffness and strength of the native and mutant lamin A/C homodimeric forms by steered molecular dynamics (SMD), a computational technique in which external forces are applied to manipulate biomolecules to probe their mechanical functions, as well as to accelerate processes that are otherwise too slow to model.[9] Among the several computational methods available, molecular dynamics (MD) is one of the most powerful. Indeed, since their pioneering applications in the late 1970 s, *in silico* protocols based on MD simulations have been extensively applied to investigate fundamental issues in protein dynamics (for recent reviews on the subject, see[10–16]).

The interactions between LINC components and integrins (cytoplasmic transmembrane receptors), desmin (intermediate filaments protein), and β-catenin (key protein of the Wnt pathway involved in cell adhesion) underline the complex mechanisms regulating the mechano-sensing and mechano-transduction processes. Recent data show that cytokine cascades induced by p38 MAPK pathway activation are implicated in several cardiovascular diseases.[17] In addition, p38 MAPK may be involved in many aspects of cardiac pathology, independent of the well-described inflammatory cytokine and chemokine pathway interactions, including gene regulation, interstitial remodeling, and endothelial dysfunction.[18,19] Indeed, p38 inhibition decreases cardiomyocyte apoptosis and improves cardiac function after myocardial ischemia and reperfusion[20] and reduces hypertrophy and left ventricular dysfunction in cardiomyopathic hamsters.[21] Conversely, p38 activation produces negative inotropic and restrictive diastolic effects thus confirming a role of this pathway in the development of both ventricular diastolic and systolic remodeling.[22] Importantly, hyperactivation of p38α has been detected in heart tissue in humans with dilated cardiomyopathy (DCM) caused by *LMNA* mutation[23] as well as in two well-known mouse models of *LMNA*-related DCM.

Due to the pivotal role of p38 MAPK pathway in many cardiac diseases and especially in dilated cardiomyopathy induced by *LMNA* alterations, ARRY-371797, a drug known to inhibit this pathway with nanomolar potency and good selectivity was used in the current study and the cells' biomechanical parameters evaluated for recovery from the biomechanical defects induced by each *LMNA* mutation.

2. Methods

2.1 Isolation and culture of ventricular cardiomyocytes from neonatal rat

Animal care and treatment were in accordance with the Italian and UE laws (*D. Lgs n° 2014/26, 2010/63/UE*). For details, see Supplementary material online.

2.2 Isolation adenoviral constructs and infection

Shuttle constructs were generated in Dual CCM plasmid DNA containing GFP gene and human LMNA cDNA, driven by two different CMV promoters to identify cells expressing LMNA protein using GFP as a marker of cellular infection. Constructs contained either human wild-type or the human mutant LMNA genes. neonatal rat ventricular myocytes (NRVMs) were infected by adenoviruses at 25 multiplicity of infection (MOI) in serum free medium; 6-h post-infection, complete medium was replaced to cardiomyocytes. More details in Supplementary material online.

2.3 Immunofluorescence

NRVMs were fixed in PBS containing 4% PFA for 20 min and permeabilized with 1%Triton X-100 for 30 min. After blocking, cells were incubated with Alexa Fluor 594 Phalloidin (Life Technologies) at 1: 500 dilution for 45 min in PBS. Each slide was mounted in Vectashield with DAPI (Vector Labs) to counter-staining the nuclei. Representative immunofluorescence images were acquired by using NIKON A1 plus Confocal microscope (NIKON Eclipse Ti), equipped with Plan-Apochromat 60X/1.40 oil objective. In order to obtain complete 3 D reconstructions of NRVM, 25 images were acquired for a total extension of 8.5 μm on the *z*-axes. More details in Supplementary material online.

2.4 ARRY-371797 administration

Following 24 hours of cardiomyocytes isolation, ARRY-371797 was administrated to the cell culture. Cells were treated in triplicate with fresh complete medium supplemented with ARRY-371797 in a final concentration of 0.1 and 1 μM in DMSO diluted incubated at 37 C for 3 hours, and then used for AFM experiments or fixed for immunofluorescence analysis.

2.5 Molecular modeling

All steered molecular dynamics (SMD) simulations and the relevant analysis were carried out using NAMD (v. 2.10) and the CHARMM22 force field[7] on our own CPU/GPU calculation cluster (see Supplementary material online for full computational details).

2.6 AFM—single cell force spectroscopy

An AFM Solver Pro-M (NT-MDT, Moscow, Russia) was used to acquire morphology as well as force–displacement curves. Sample preparation, and measurements are detailed in Supplementary material online.

2.7 Modeling cells elasticity

The Young's modulus (elasticity) is often used to describe mechanical properties of cells. The prevalent method of evaluating AFM indentation data to assess the elasticity is the so-called 'Hertz-Sneddon model' of contact between two elastic bodies. Model and equation used are detailed in Supplementary material online.

2.8 Plasticity index

To characterize the relative elastic-plastic behavior of the cell during the AFM loading/unloading we used the plasticity index ζ parameter. Model and equation used are detailed in Supplementary material online.

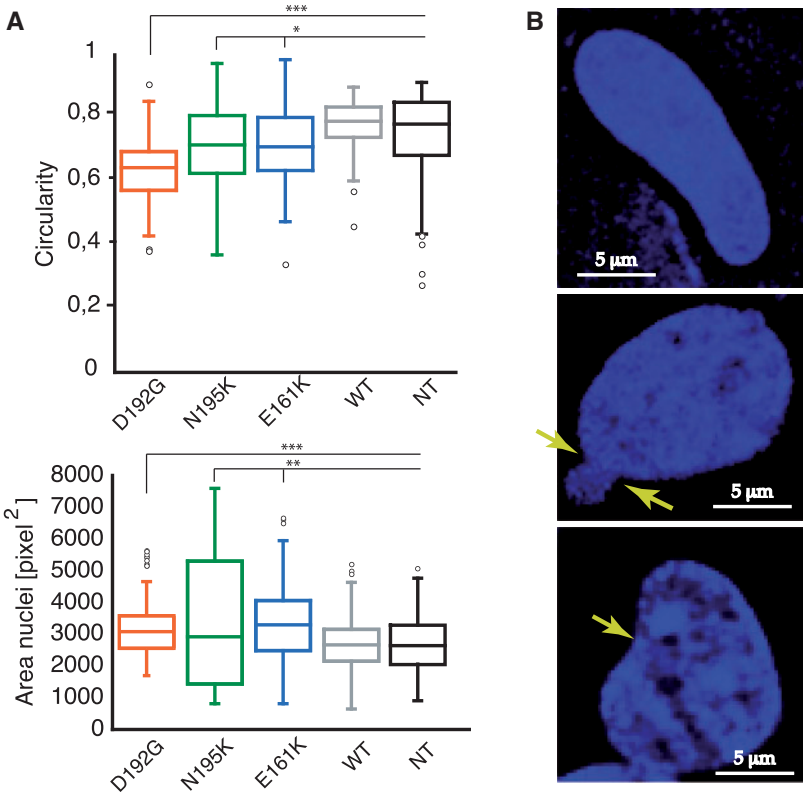

Figure 1 Nuclear malformations in mutant NRVM. Panel *A*: analysis of nuclear circularity and nuclear area, showing abnormally shaped and larger mutant nuclei. At least 100 nuclei were analysed. The normality of the data has been tested with the Shapiro–Wilk normality test. Since the data do not have a normal distribution we applied a non-parametric test (Kruskal–Wallis) and since this test was significant, a *post hoc* analysis (Dunn's test, confidential level alpha = 0.05) was performed. ***Represents $P < 0.0001$, ** $P < 0.001$ (*t*-test). Panel *B*: arrows show examples of alterations in nuclear morphology, elongated, blebs, and misshapen nuclei.

2.9 Statistics

Experimental AFM data were analysed using GraphPad Prism software. All data were first subjected to Shapiro normality test and then ordinary one-way ANOVA with Holm–Sidak's multiple comparisons test for normal distributions or the Kruskal–Wallis test with a Dunn's multiple comparisons test otherwise, both with a two-tailed *P* value, were employed. Data in the text are reported as mean (normal distribution) or median (non-normal distribution) values ± SE. More details see Supplementary material online.

3. Results and discussion

The *LMNA* mutations were selected because they represented a recurrent mutation (E161K[24–26]), a mutation associated with visible disruption of nuclear envelope morphology (D192G[27]), and one of the originally reported *LMNA* cardiomyopathy mutations (N195K[28]). The E161K mutation was also present in three families from our Familial Cardiomyopathy Registry population (unpublished; see Supplementary material online, *Figure S1*). Combining our cases with those in the literature yielded clinical data on 16 individuals who carry the E161K mutation with an average age of symptom onset for dilated cardiomyopathy and death/cardiac transplantation of 40.8 (±15.3) and 40.0 (±8.7) years, respectively. None of the patients had signs of skeletal muscle involvement, and the overall prognosis appeared relatively mild with 12.5% of patients dying or requiring transplant by age 40 years. In contrast, the D192G mutation has been described in one family with a severe phenotype where symptom onset and death/transplantation occurred at 30.5 (±6.4) and 32.0 (±7.1) years, respectively: both patients died before the age of 40 years.[29] The initial report, along with follow-up studies noted severe ultrastructural disruption of nuclear envelope architecture,[30,31] findings that could suggest perturbed nuclear or cellular biomechanics. The N195K mutation was reported in the initial seminal paper by Fatkin et al.[32] and then again by van Tintelen et al. in 2007,[33] providing data on 17 affected patients with a high frequency of arrhythmias and sudden death (58.8% death or transplant by age 40 years) and symptom onset and death/transplantation occurring at 26.0 (±8.9) and 37.2 (±7.5) years, respectively. Although the small number of observations of these rare mutations must be taken into consideration, clinical data suggest that *LMNA* D192G and N195K have a more severe outcome compared with E161K (Fisher's exact test, $P = 0.0027$ for the events of death or heart transplant before age 40 years).

3.1 Immunofluorescence

Microscopy analysis showed that D192G and N195K mutant cardiomyocytes frequently exhibited nuclear malformations, less frequently also E161K showed some malformations. Typical examples of alterations, specifically elongated, blebs, or misshapen nuclei, are indicated in *Figure 1*, right panel. The nuclear circularity of control and mutant NRVMs was quantified by image analysis. The mean circularity was

significantly lower for mutant cells compared with NT and WT cardiomyocytes (*Figure 1*, left panels). Furthermore, the nuclei of these cells showed aggregates of different sizes and distributions, in agreement with prior reports.[34–37] Aggregates were rare in the wild-type (WT) cells (<10% of nuclei contained them) and the aggregates area was 14.8% ± 2.7. The percentage of aggregates was highest in the case of both D192G (>95% of nuclei with an area of 29.6% ± 8.7), and N195K (>95% with an area of 25.9% ± 4.48) and progressively lower in E161K (<50% with an area of 16.1% ± 3.4). Furthermore, the nuclei with the highest density of aggregates also showed a disorganized cytoskeleton actin network (*Figures 2* and *3A* and see Supplementary material online, *Figure S2*). The differences in actin network are also highlighted by the fluorescence relative intensity showed in *Figure 3B*.

3.2 Molecular modeling

Figure 4A shows the deformation of WT and mutant LMNA dimer structures described by stress–strain curves at the pulling speed of 1 m/s. In line with previous findings on other intermediate filament dimeric proteins,[38] our simulations identify three distinct regions of deformations in the corresponding plots. The first region of these plots, also seen in actual measurements,[39] corresponds to an elastic regime (regime I), in which the stress increases linearly with the applied strain. A plateau region during which the stress remains approximately constant with increasing deformation (regime II) follows. This part of the stress–strain curve corresponds to the unfolding of the protein α-helical domains, and it begins at the so-called angular point, that is the value of strain at which a significant change in the curve derivative is observed. Of note, the very slight increase of the stress in regime II, particularly towards the end of this region, can be ascribed to the fact that, as more and more turns in the α-helices become unfolded, higher forces are required to produce more protein unfolding since the failure probability decreases with decreasing number of remaining helical turns.[40] Finally, in the last part of the curve, (regime III) the stress steadily increases due to the pulling of the unfolded backbone of the protein, the stretching of covalent bonds ultimately leading to substantial increase in stiffness. Other similar experimental and simulated mechanical behaviors (in terms of stress–strain curves and unfolding force levels) have been reported in literature for other coiled-coil intermediate filament protein dimers,[41] consistent with the present results.

A comparison of the curves in panel A of *Figure 4* reveals that no meaningful differences in either the stress–strain data or the unfolding dynamics between LMNA WT and E161K can be observed. This is also confirmed by the magnification of the small deformation regime (*Figure 4B*), supporting the notion that the behavior of these two protein forms is almost superimposable in the low deformation range, which is the closest to the one experienced by the intermediate filaments *in vivo*. In contrast, LMNA N195K and, to a greater extent, LMNA D192G dimers exhibit a different behavior with respect to the WT. In particular, the stress–strain profile of the D192G mutant appears to enter regime II somewhat earlier with respect to the native LMNA WT and the force and hence stress value characterizing this regime is lower than those estimated for all other proteins analysed. This qualitative observation is confirmed by the data in *Table 1*. These data are referred as regime I, where all protein dimers are deformed homogeneously before the unfolding process sets in.

As seen in *Table 1*, unfolding for all proteins is predicted in a narrow range of strain values, slightly decreasing in the order D192G (13%), WT (14%), E161K (15%), and N195K (16%). However, the corresponding stress values at the angular points are significantly different, and range from 40.6 MPa for LMNA D192G to 62.8 MPa for E161K. Notably, however, this translates into comparable values of the calculated E_D values for the WT and E161K LMNA dimers (412 and 421 MPa, respectively), while for the other two mutants this value decreases significantly to 362 MPa and 302 MPa for LMNA N195K and D192G, respectively. Importantly, these simulated values are in agreement with both experimental and calculated results reported for a closely related intermediate filament, vimentin. Indeed, experimental data for vimentin are in the range 300–900 MPa[42] while simulations predicts *E* values between 380 and 540 MPa (depending on different pulling rate, 300 MPa being obtained at the same pulling rate adopted in the present study[41]).

An analysis of simulated conformation structures generates a potential model for the protein deformation mechanism. *Figure 4C* shows different predicted conformations for dimeric LMNA protein under a steered molecular dynamics simulation stretching pathway.

In the initial stage of the simulation, where the applied deformations are small, the entire dimeric protein structure first aligns along the pulling direction and then the α-helical coiled-coil domains stretch slightly to counteract deformation and to accommodate the corresponding elongation. In agreement with data reported in *Table 1*, no molecular rupture or protein unfolding is seen up to the corresponding yield strain (regime I, *Figure 4A*), after which the α-helical segment begins to unwind and formation of β-sheet domains is observed (regime II). This phenomenon, experimentally verified[39,43,44] and known as α–β transition, corresponds to the plateau region in *Figure 4A*. As the strain is further increased (>100%), the secondary super-helical configuration is lost and additional pulling results in the stretching of the protein covalent bonds. This eventually translates into the rapid increase of the relevant stress–strain curve (regime III, *Figure 4A*).

3.3 Single-cell force spectroscopy

To study the effect of *LMNA* mutations on cardiomyocytes *in vitro*, we used our established model of NRVMs infected with an adenoviral construct carrying either the WT or the mutant E161K, D192G, or N195K *LMNA* cDNA as well as the Enhanced Green Fluorescent Protein (EGFP) used to identify LMNA expressing cells.[45,46] At day 1 after infection, the Young's modulus obtained from the AFM-SCFS tests, an indicator of nuclear elasticity, did not change under different conditions, in agreement with our previous work.[45,46] In contrast, at day 2 after infection, the results for the three mutant cell subsets were statistically different from uninfected, 'non-treated' NRVM (NT) and WT cells.

Data shown in *Figure 5A* are those obtained after 2 days from the adenoviral infection and indicate that, while NT and WT elasticity remained similar, the Young's modulus in cells expressing mutant LMNA diverged significantly from both NT (1.47 ± 0.009 kPa) and WT (1.44 ± 0.008 kPa). More precisely, D192G displayed the highest Young Modulus (3.03 ± 0.27 kPa) followed by N195K (2.55 ± 0.13 kPa) and E161K (2.14 ± 0.10 kPa). A comparison among the three mutations shows that the N195K is 16% and the E161K is 30% less stiff than the D192G, respectively.

SCFS curves contain additional information about the biomechanical response of a cell towards external mechanical stimuli. Specifically, the three mutations exhibit evident effects on the work of adhesion required to detach the spherical tip of the AFM cantilever from the cell membrane after indentation. As shown in *Figure 5B*, adhesion work was lower for all mutations compared to NT and WT. As for the elasticity, similar to the effects on adhesion, LMNA D192G NRVMS are the most affected with a reduction of 45% of adhesion compared to the NT (3.29 ± 0.28 fJ vs. 1.81 ± 0.16 fJ). This confirms that these deleterious effects extend

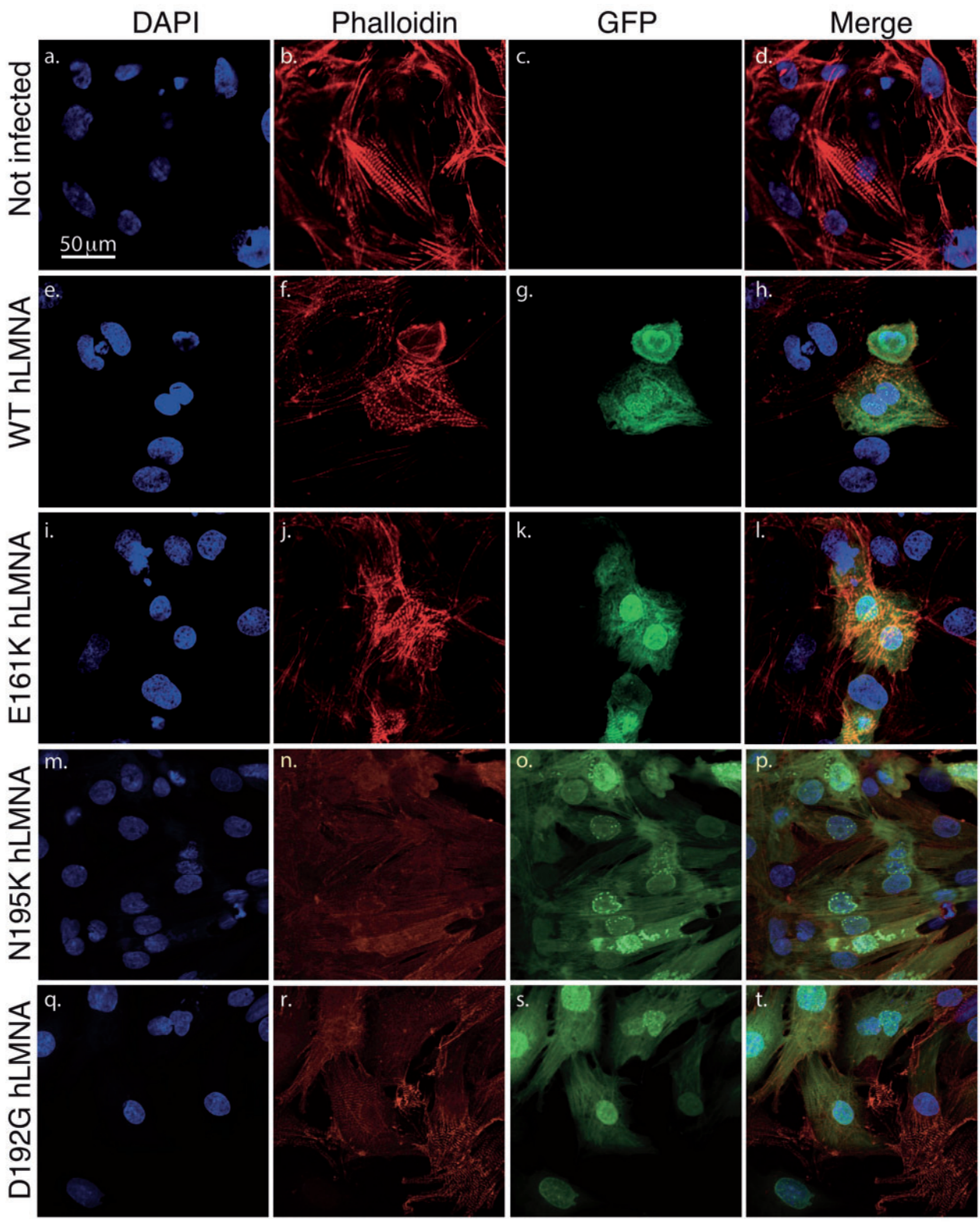

Figure 2 Some Lamin A mutants have a dramatically abnormal intranuclear localization. Cellular localization of human EGFP-AdV-WT-LMNA and mutants (E161K, D192G, N195K). Laser scanning confocal immunofluorescence microscopy images of NRVMs cells stained for actin-stress fibers with phalloidin, (F-Actin) (red left-middle column) and GFP (green, right middle column). The nuclei are stained in DAPI (blue, left column). Right column: an overlay of the three channels. Particularly evident appear the intranuclear blebs in N195K mutant cells, visible also in E161K and D192G. Bar 50 µm ($n = 4$).

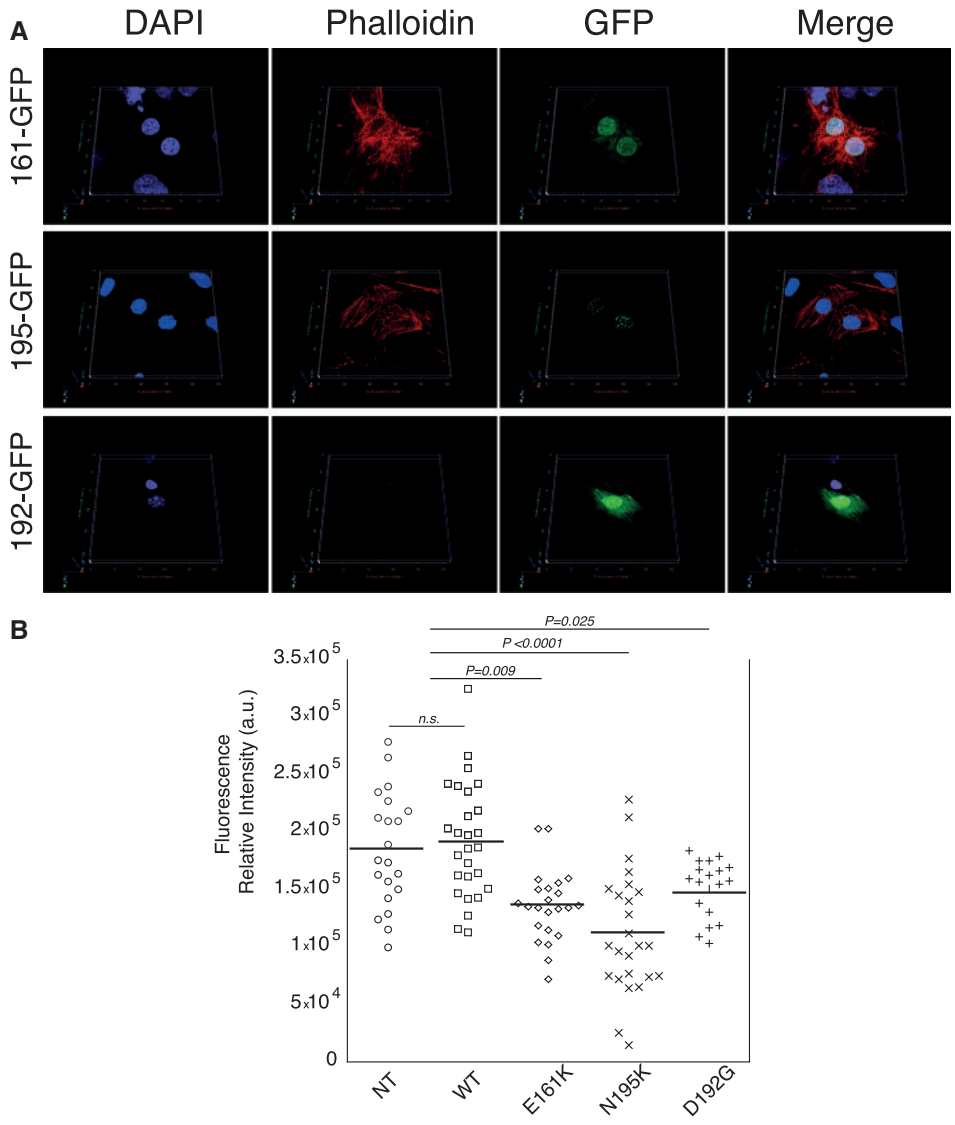

Figure 3 Mutant cells display cytoskeletal alteration in NRVMs. Panel *A*: Representative images of fluorescently stained actin cytoskeleton of mutant cells. Cells were stained with fluorescent phalloidin (which specifically stains F-actin, red). Extensive cytoskeletal network alteration was evident. For base reference (NT and WT) see column 2 of *Figure 2*. Scale bar 50 μm. Panel *B*: Actin relative fluorescence intensity for mutant cells compared to NT and WT ($n = 4$).

beyond the increased nuclear stiffness, to include defective cell membrane adhesion work.

At the same time, cells expressing any of the three mutations are more viscous compared to NT cells, being able to store less elastic energy in their cytoskeleton components if subjected to a rapid mechanical stress as shown by the plasticity index data (*Figure 5C*). Again, LMNA D192G shows the most obvious effects (0.46 ± 0.01 vs. 0.36 ± 0.1 for NT). These results could be associated with a lower resistance to deformation due to a non-optimal transmission of mechanical stresses from the membrane to the nucleus due to a defective actin structure.[45]

3.4 Pharmacologic rescue of NRVM biomechanical properties

Understanding the disease mechanisms and the possibility of rescue is critical for the development of novel therapies. Currently, there are no specific therapies for *laminopathies*, and treatment guidelines for lamin-related DCM follow general recommendations for treatment of HF and prevention of SCD. Advanced strategies to develop novel treatments include repurposed molecularly directed drugs, which at present are probably the most realistic approach. In animal models of *LMNA*-associated DCM, activation of the mTOR pathway has been reported, and, inhibition of mTOR by temsirolimus or rapamycin is able to rescue the DCM phenotype.[47,48] The mitogen activated protein kinase (MAPK) pathway signaling which, is activated by stress, in particular oxidative stress, and is involved in cell senescence, is increased in *LMNA*-associated DCM. There is increasing evidence for a pivotal role of p38 MAPK, in particular, in a variety of disease including cardiovascular dysfunction.[19,21] Recently, activation of the p38 MAPK pathway has been linked to aberrant cardiovascular function in patients with dilated cardiomyopathy (DCM) due to lamin A/C (LMNA) gene mutations.[49] Recently, encouraging results were reported from a Phase 2 pilot clinical trial of ARRY-371797

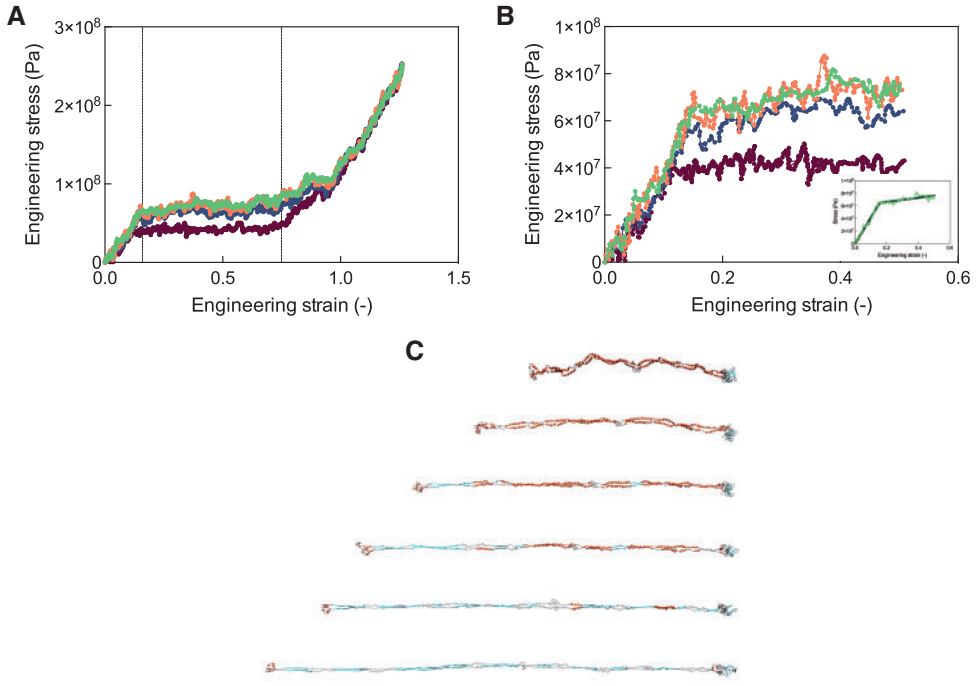

Figure 4 Molecular dynamics simulations of mutant LMNA. (*A*) Simulated stress–strain curves at pulling speed 1 m/s for wild type and mutant LMNA dimers: green, WT; orange, E161K; blue, N195K; dark red, D192G. The three different regimes in the stress–strain behavior are marked by the two vertical dotted lines: regime I: left-hand side of the curve up to first vertical line, regime II: between first and second dotted line, regime III: from second dotted line on. (*B*) Zoomed view of the small deformation regime of the stress–strain curves shown in (*A*). The insert illustrates the tangent method used to estimated (i) the slope in the elastic region namely the dimer Young Modulus (E_D), (ii) yield stress, and (iii) yield strain (see *Table 1*). (*C*) Simulated conformational structures of the LMNA dimer structure under tensile loading (pulling rate 1 m/s). Upon increasing strain (from top to bottom: 0%, 25%, 50%, 75%, 100%, and 125%), the α-helical content (red) of LMNA progressively decreases while β-sheet domains (cyan) are formed.

Table 1 Values of the dimer Young's modulus *ED*, yield strain, and yield stress obtained with the tangent method from the simulated data reported in *Figure 4B*

LMNA Protein	Dimer Young's modulus *ED* (MPa)	Yield strain (-)	Yield stress (MPa)
WT	412	0.14	57.7
E161K	421	0.15	62.8
N195K	362	0.16	56.6
D192G	302	0.13	40.6

The insert in *Figure 4B* shows the method applied to LMNA WT as an example.

(Array Biopharma, Boulder, CO), an oral, selective p38 MAPK inhibitor in 12 patients with *LMNA*–associated DCM (ClinicalTrials.gov NCT02057341), and this compound has been selected for our investigations.

To explore if the altered biomechanical properties of NRVMs carrying the three LMNA mutations could be recovered, mutant and control cells were subjected to a treatment with ARRY-371797.

Two concentrations were used, 0.1 and 1.0 μM, which as shown in Supplementary material online, *Figure S3*, do not change the Young Modulus of the NT cells, and represent concentrations that are achievable *in vivo*. *Figure 6A–C* are the Young modulus, the adhesion work and the plasticity index calculated after the rescue experiment, respectively. The rescued cells showed values similar to those of NT and WT; even at the lower concentration evaluated (*Figure 6*). p38 MAPK has been hypothesized to interact with the actin cytoskeleton via the MAPK-activated kinase-2. Both actin and p38 MAPK have been suggested to play a role in the regulation of cell growth, differentiation and apoptosis in cardiomyocytes.[50] Lastly, disruption of actin-filament integrity has been shown to play a role in the initiation of cardiomyocyte apoptosis.[51] Thus, loss of functional actin may lead to decreased contractility, and also cell death by apoptosis, and ultimately disruption of the kinetics of the entire myocardium.[52] In order to verify if alterations of the actin cytoskeleton were induced by the LMNA mutations, and subsequently reversed by ARRY-371797 treatment, additional immunocytochemistry experiments were performed to assess actin distribution. Confocal microscopy images showed that in control NRVMs and NRVMs expressing WT LMNA, actin microfilaments appeared to be highly organized and homogeneously distributed (*Figure 7A*). On the contrary, mutants NRVMs were characterized by attenuation and clear disarray of the actin microfilaments (*Figure 7A*). Furthermore, a quantitative measurement of actin fluorescence relative intensity showed a significant reduction of this cytoskeletal component in all mutant cells compared to NT and WT (*Figure 7B*). However, an almost complete recovery of this cytoskeleton component was documented after treatment with ARRY-371797 (P = n.s. compared to CT and WT) (*Figure 7B*).

It is well known that different diseases caused by *LMNA* mutations can have very different effects on cellular and nuclear mechanics. Several, but

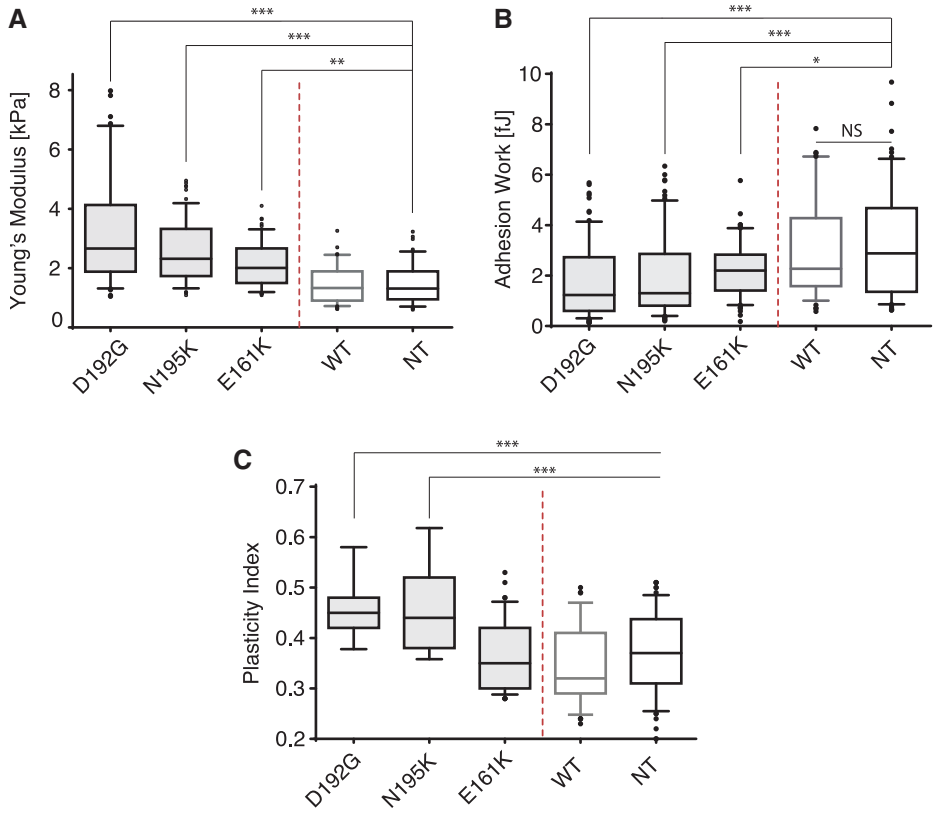

Figure 5 Altered biomechanics in *LMNA* mutant NRVMs. (*A*) Elasticity (Young Modulus) for the mutations compared to control (NT) and wild-type (WT). (*B*) Adhesion work for the three mutations. The work of adhesion reflects the process of detachment of the cardiomyocyte cell membrane (the sarcolemma) to the AFM tip. (*C*) Viscoelasticity described by the plasticity index. (*** $P < 0.0001$, ** $P < 0.001$, * $P < 0.05$). (independent experiments, $n = 7$ for NT and WT, $n = 8$ for every mutation. Number of cells, $N = 51$ NT, 47 WT, 56 E161K, 65 N195K, 42 D192G).

not all, mutations causing muscular dystrophy and dilated cardiomyopathy reportedly show an increased nuclear deformability,[53] while the Hutchinson–Gilford progeria Δ50 *LMNA* mutation results in increased nuclear stiffness.[54,55] Generally, cell mechanical behavior can be broken down into two main components: (i) the nucleus and (ii) the cytoskeleton. However, response of the nucleus is due to: (i) the elastic lamina, which has an elastic modulus much higher than the cell membrane[56] and (ii) the viscoelastic chromatin.[57–59] When mechanical stresses are applied to the cell, nuclei undergo a rapid, elastic, deformation with a subsequent viscoelastic contribution on a time-scale of seconds.[60] The molecular modeling experiment that we have carried out cannot take into consideration all these cell components, however the results of both molecular modeling and AFM-SCFS show a similar trend in the changes of biomechanical properties of the three *LMNA* mutations. This is remarkable considering that the data calculated using molecular modeling are obtained only from the LMNA dimers, while the AFM data reflect the complexity of the cell structure including the contribution of nuclear wall, chromatin, and cytoskeleton structures. In this regard, it is worth mentioning that a small fraction of lamin proteins (~10% of A-type lamins) also locates within the nuclear interior, where lamins intermingle with nuclear binding partners.[61,62] It is possible that nucleoplasmic lamins also contribute to the overall stiffness, possibly by forming a framework or by influencing global chromatin structure. Furthermore, all three mutations showed different amounts of aggregates, previously identified as heterochromatin,[28,63] randomly distributed within nuclear matrix forming dense clumps. Although we cannot rule out that the aggregate formation may in part be due to the exogenous LMNA expression, our data, in line with a series of other investigations, show that abnormal nuclear morphology and aggregates are the result a LMNA mutations specific effect.[27,45,64,65]

Remarkably, the alteration of the nuclear shape is generally associated with senescence that is characterized by changes in chromatin structure and subsequent formation of heterochromatic foci. In fact, the most severe premature ageing syndromes, such as Hutchinson Gilford's syndrome or atypical Werner's syndrome, are associated with alterations of the nuclear shape resulting from the deregulation of lamin A/C. Interestingly, silencing of p38 MAPK in human fibroblasts characterized by ataxia telangiectasia also led to a reduction in the frequency of cells with alterations in nuclear shape and concomitantly to a reduction in the frequency of senescent cells.[66] Furthermore, in mice with LMNA mutations, there is a loss of functional lamin proteins leading to p38 MAPK pathway activation with subsequent structural changes in cardiac tissue. In these mouse models, treatment with MAPK inhibitors improves abnormal nuclear shape and sarcomere structure.[23,67]

In our investigations using MD and AFM methods, the D192G mutation produced the most detrimental changes in NRVMs. On the other hand, the E161K mutation, consistently displayed the mildest biomechanical changes, Lastly, biomechanical characteristics associated with

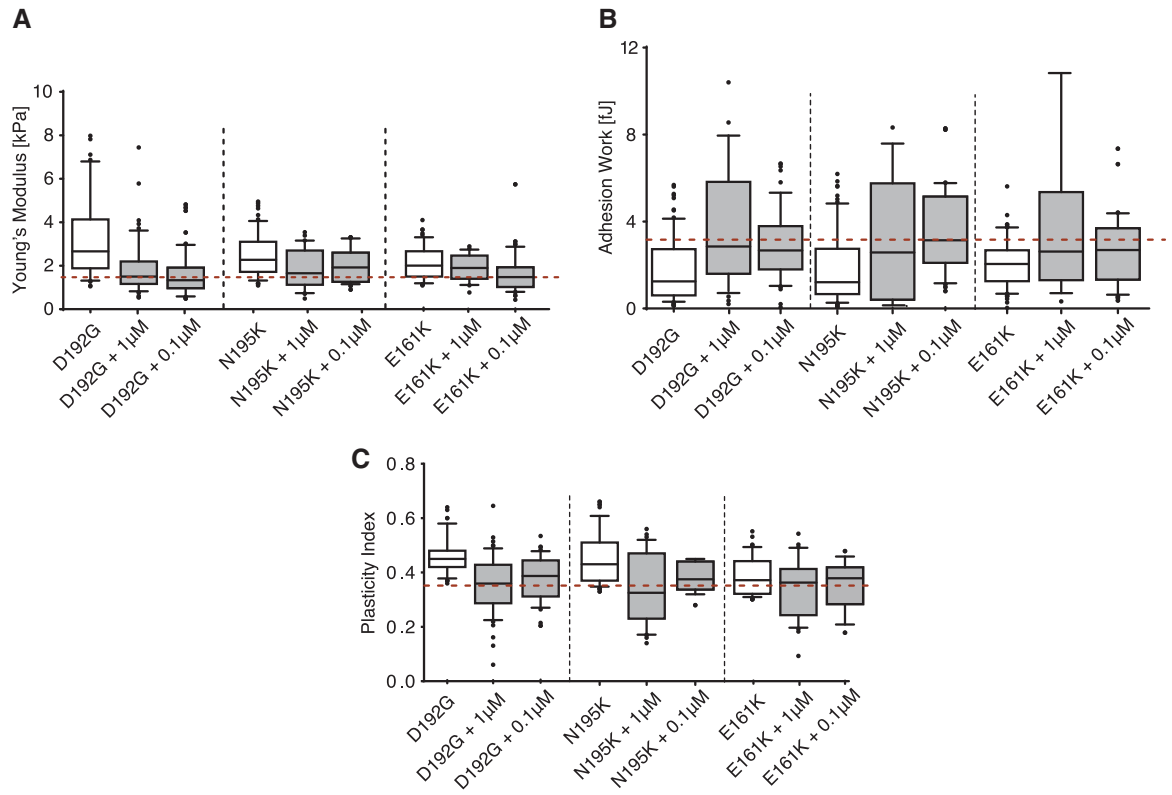

Figure 6 Pharmacological rescue of biomechanical defects in *LMNA* mutant NRVMs. (*A*) Elasticity (Young Modulus) of mutant and control NRVMs before (empty boxes) and after (full boxes) treatment with 0.1 and 1 μM of ARRY-371797. Red dotted line is the value of the Young Modulus for the NT cells. (*B*) Adhesion work before (empty boxes) and after (full boxes) 0.1 and 1 μM of ARRY-371797. Red dotted line is the value of the adhesion work for the NT cells. (*C*) Plasticity index before (empty boxes) and after (full boxes) 0.1 and 1 μM of ARRY-371797. Red dotted line is the value of the plasticity index for the NT cells. (independent experiments, $n = 6$. Number of cells, $N = 51$ NT, 47 WT, 56 E161K, 65 N195K, 42 D192G).

the N195K mutation were always intermediate between the other two mutations yet more similar to the D192G mutation. For the E161K mutation, it was shown[7] that the1B dimer unfolds at similar force range compared to the wild type and therefore this mutant dimer has elastic properties comparable to those of the wild type. However, both the stress applied on the nucleus through the AFM or the orientation of the dimer due to the fibrous nature of lamina network in cells could not be correlated directly with mechanical unzipping experiments using single-molecule force spectroscopy nevertheless, both our data (MD and AFM) confirm that E161K mutation does not have a significant impact on its mechanical properties.

In this regard, it is important to highlight that in the D192G mutation, glycine, a nonpolar hydrophobic amino acid, substitutes an aspartic acid, a negatively charged polar and hydrophilic amino acid. This substitution is disfavored and has a significant impact on the LMNA protein biomechanical properties. The N195K mutation has an asparagine, a polar amino acid, substituted by a lysine, a positively charged polar amino acid. This substitution is chemically less disfavored. Finally, the E161K mutation has a glutamate, a polar negatively charged amino acid, substituted by a lysine which is positively charged. Lysine is frequently involved in salt-bridges, where it couples with a negatively charged amino acid to create stabilizing hydrogen bonds and this could affect LMNA protein stability.

3.5 Study limitations

It should be noted that data generated in NRVMs, although a well-established *in vitro* cardiomyocyte model, may not fully translate in the biomechanical behavior of adult cardiomyocytes embedded in the muscle tissue.

3.6 Conclusions

In our study, MM and AFM-SCFS have been employed to advance our understanding of the mechanisms underlying nuclear LMNA functions, as well as the effects of *LMNA* mutations. AFM findings support the molecular modeling results, suggesting that all three mutations generate distinctive structural changes. Interestingly, even though molecular modeling considered only the deformation of single dimers and AFM examined the whole cell, both sets of data rank the effects of the three mutations consistently, predicting that *LMNA* D192G will be the most damaging, followed by N195K and E161K. Remarkably, biomechanical findings are in agreement with clinical findings and even though, genotype-phenotype correlation was evaluated in an extremely limited population, data suggest that the most severe outcome is associated with the D192G variant, while the mildest with the E161K. Finally, we showed that ARRY-371797, a p38 MAPK pathway inhibitor, was able to rescue the biomechanical properties for all three LMNA mutant

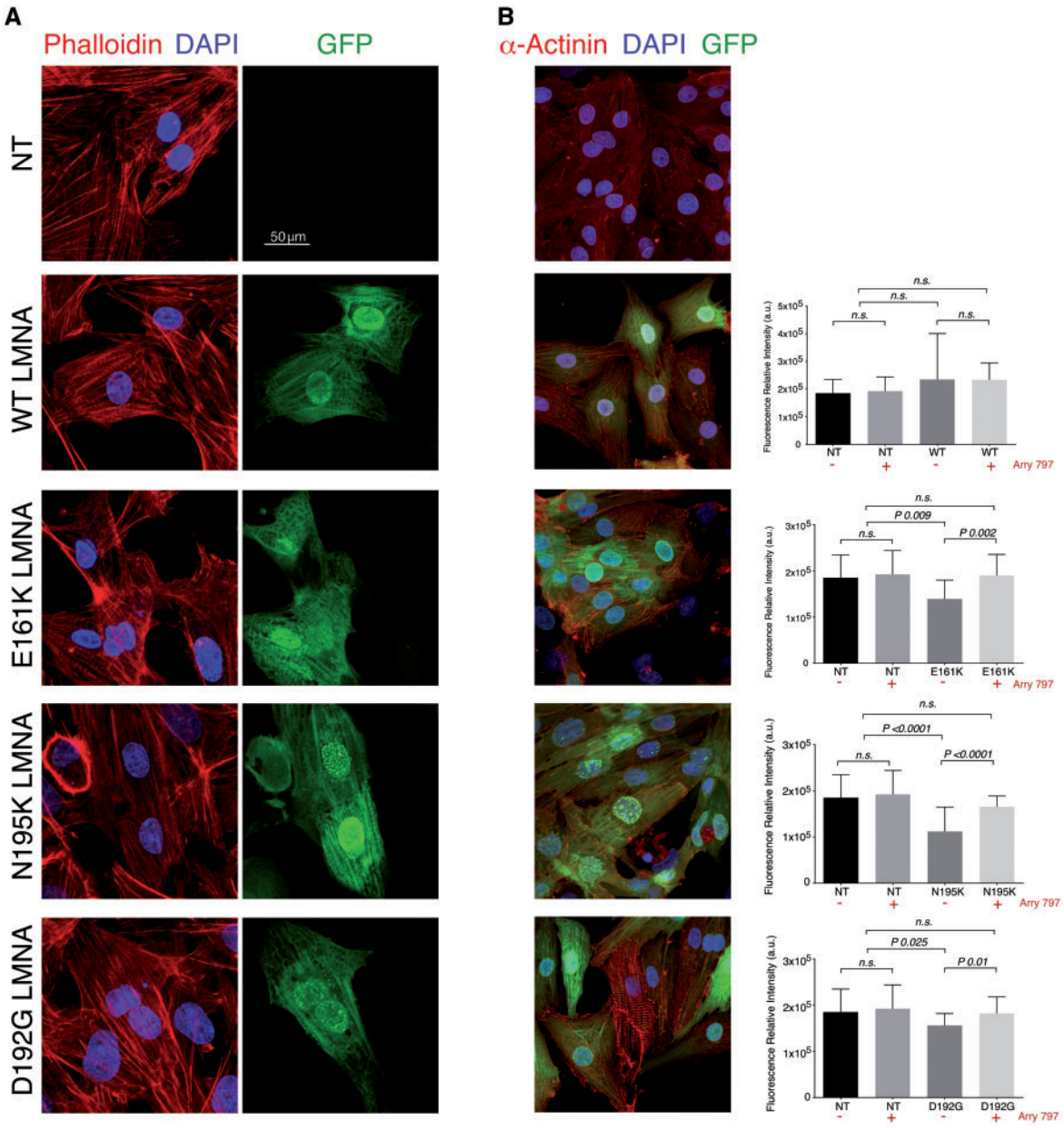

Figure 7 ARRY-371797 treatment restores actin network altered by LMNA mutations. (*A*) Confocal microscopy of actin cytoskeleton network in control NRVMs (NT) and after adenovirus infection with GFP-WT, and mutant-GFP LMNAs (E161K, N195K, D192G). Alexa 594-labeled phalloidin (red) was used to examine F-actin under basal condition (NT, vehicle only), or after 3 h incubation with 0.1 mM of ARRY-371797. (*B*) Immunofluorescence panels showing the expression of sarcomeric alpha-actinin (red) and EGFP-AdV-LMNA constructs (green) after ARRY-371797 treatment. Data show a significant increase of fluorescence in mutant NRVMs treated with ARRY-371797 compared to non treated NRVM cells. Scale bar in A = 50 µm. All images were acquired under identical conditions (independent experiments, $n = 4$).

cardiomyocytes and generate a good recovery of the actin network, providing further supportive data for the clinical evaluation of this compound in *LMNA*-related DCM and supporting the role of AFM-SCFS as a biomarker *in vitro* for novel drugs screening.

Supplementary material

Supplementary material is available at *Cardiovascular Research* online.

Author's contributions

The manuscript was written through contributions of all authors. All authors have given approval to the final version of the manuscript. O.S., L.M., M.R.G.T., C.S.L., and S.P. designed research studies, E.L., V.M., L.P., D.B., and T.L. conducted experiments, acquired data, and analysed data, P.L. provided reagents, O.S., L.M., E.L., S.P., and M.R.G.T. drafted, and wrote the manuscript.

Conflict of interest: L.M. and M.R.G.T. are consultants to Array Biopharma. P.L. is an employee of Array Biopharma. Other authors have declared that no conflict of interest exists.

Funding

This study was supported by the following grants: NIH UL1 RR025780 (L.M.), NIH UL1 TR001082 (L.M.), NIH R01 HL69071 (L.M.), R01 HL116906 (L.M.), NIH K23 JL067915 (M.R.G.T.), NIH R01HL109209 (M.R.G.T.); Trans-Atlantic Network of Excellence grant from the Leducq Foundation (14-CVD 03) (O.S., L.M., and M.R.G.T.). Moreover, it was financially supported by the Research Fund of the University of Trieste (FRA 2016 project) '*In silico/in vitro* combined study of biomechanical and molecular alterations induced by Lamin protein mutations and detection of specific miRNAs as Biomarker for idiopathic dilated cardiomyopathy' (S.P., E.L. and O.S.).

References

1. Cattin ME, Muchir A, Bonne G. 'State-of-the-heart' of cardiac laminopathies. *Curr Opin Cardiol* 2013;**28**:297–304.
2. Worman HJ, Ostlund C, Wang Y. Diseases of the nuclear envelope. *Cold Spring Harb Perspect Biol* 2010;**2**:a000760.
3. Dhe-Paganon S, Werner ED, Chi YI, Shoelson SE. Structure of the globular tail of nuclear lamin. *J Biol Chem* 2002;**277**:17381–17384.
4. Stuurman N, Heins S, Aebi U. Nuclear lamins: their structure, assembly, and interactions. *J Struct Biol* 1998;**122**:42–66.
5. Burkhard P, Ivaninskii S, Lustig A. Improving coiled-coil stability by optimizing ionic interactions. *J Mol Biol* 2002;**318**:901–910.
6. Strelkov SV, Herrmann H, Geisler N, Wedig T, Zimbelmann R, Aebi U, Burkhard P. Conserved segments 1A and 2B of the intermediate filament dimer: their atomic structures and role in filament assembly. *EMBO J* 2002;**21**:1255–1266.
7. Bera M, Ainavarapu SR, Sengupta K. Significance of 1B and 2B domains in modulating elastic properties of lamin A. *Sci Rep* 2016;**6**:27879.
8. Szeverenyi I, Cassidy AJ, Chung CW, Lee BT, Common JE, Ogg SC, Chen H, Sim SY, Goh WL, Ng KW, Simpson JA, Chee LL, Eng GH, Li B, Lunny DP, Chuon D, Venkatesh A, Khoo KH, McLean WH, Lim YP, Lane EB. The Human Intermediate Filament Database: comprehensive information on a gene family involved in many human diseases. *Hum Mutat* 2008;**29**:351–360.
9. Isralewitz B, Gao M, Schulten K. Steered molecular dynamics and mechanical functions of proteins. *Curr Opin Struct Biol* 2001;**11**:224–230.
10. Palamini M, Canciani A, Forneris F. Identifying and visualizing macromolecular flexibility in structural biology. *Front Mol Biosci* 2016;**3**:47.
11. Karshikoff A, Nilsson L, Ladenstein R. Rigidity versus flexibility: the dilemma of understanding protein thermal stability. *FEBS J* 2015;**282**:3899–3917.
12. Ostermeir K, Zacharias M. Advanced replica-exchange sampling to study the flexibility and plasticity of peptides and proteins. *Biochim Biophys Acta* 2013;**1834**:847–853.
13. Micheletti C. Comparing proteins by their internal dynamics: exploring structure-function relationships beyond static structural alignments. *Phys Life Rev* 2013;**10**:1–26.
14. Teilum K, Olsen JG, Kragelund BB. Protein stability, flexibility and function. *Biochim Biophys Acta* 2011;**1814**:969–976.
15. Leone V, Marinelli F, Carloni P, Parrinello M. Targeting biomolecular flexibility with metadynamics. *Curr Opin Struct Biol* 2010;**20**:148–154.
16. Galera-Prat A, Gómez-Sicilia A, Oberhauser AF, Cieplak M, Carrión-Vázquez M. Understanding biology by stretching proteins: recent progress. *Curr Opin Struct Biol* 2010;**20**:63–69.
17. Kerkela R, Force T. p38 mitogen-activated protein kinase: a future target for heart failure therapy? *J Am Coll Cardiol* 2006;**48**:556–558.
18. Behr TM, Berova M, Doe CP, Ju H, Angermann CE, Boehm J, Willette RN. p38 mitogen-activated protein kinase inhibitors for the treatment of chronic cardiovascular disease. *Curr Opin Investig Drugs* 2003;**4**:1059–1064.
19. Petrich BG, Wang Y. Stress-activated MAP kinases in cardiac remodeling and heart failure; new insights from transgenic studies. *Trends Cardiovasc Med* 2004;**14**:50–55.
20. Ma XL, Kumar S, Gao F, Louden CS, Lopez BL, Christopher TA, Wang C, Lee JC, Feuerstein GZ, Yue TL. Inhibition of p38 mitogen-activated protein kinase decreases cardiomyocyte apoptosis and improves cardiac function after myocardial ischemia and reperfusion. *Circulation* 1999;**99**:1685–1691.
21. Kyoi S, Otani H, Matsuhisa S, Akita Y, Tatsumi K, Enoki C, Fujiwara H, Imamura H, Kamihata H, Iwasaka T. Opposing effect of p38 MAP kinase and JNK inhibitors on the development of heart failure in the cardiomyopathic hamster. *Cardiovasc Res* 2006;**69**:888–898.
22. Liao P, Georgakopoulos D, Kovacs A, Zheng M, Lerner D, Pu H, Saffitz J, Chien K, Xiao RP, Kass DA, Wang Y. The in vivo role of p38 MAP kinases in cardiac remodeling and restrictive cardiomyopathy. *Proc Natl Acad Sci U S A* 2001;**98**:12283–12288.
23. Muchir A, Wu W, Choi JC, Iwata S, Morrow J, Homma S, Worman HJ. Abnormal p38α mitogen-activated protein kinase signaling in dilated cardiomyopathy caused by lamin A/C gene mutation. *Hum Mol Genet* 2012;**21**:4325–4333.
24. Mewborn SK, Puckelwartz MJ, Abuisneineh F, Fahrenbach JP, Zhang Y, MacLeod H, Dellefave L, Pytel P, Selig S, Labno CM, Reddy K, Singh H, McNally E. Altered chromosomal positioning, compaction, and gene expression with a lamin A/C gene mutation. *PLoS One* 2010;**5**:e14342.
25. Sébillon P, Bouchier C, Bidot LD, Bonne G, Ahamed K, Charron P, Drouin-Garraud V, Millaire A, Desrumeaux G, Benaïche A, Charniot JC, Schwartz K, Villard E, Komajda M. Expanding the phenotype of LMNA mutations in dilated cardiomyopathy and functional consequences of these mutations. *J Med Genet* 2003;**40**:560–567.
26. Perrot A, Hussein S, Ruppert V, Schmidt HH, Wehnert MS, Duong NT, Posch MG, Panek A, Dietz R, Kindermann I, Böhm M, Michalewska-Wludarczyk A, Richter A, Maisch B, Pankuweit S, Ozcelik C. Identification of mutational hot spots in LMNA encoding lamin A/C in patients with familial dilated cardiomyopathy. *Basic Res Cardiol* 2009;**104**:90–99.
27. Sylvius N, Bilinska ZT, Veinot JP, Fidzianska A, Bolongo PM, Poon S, McKeown P, Davies RA, Chan KL, Tang AS, Dyack S, Grzybowski J, Ruzyllo W, McBride H, Tesson F. In vivo and in vitro examination of the functional significances of novel lamin gene mutations in heart failure patients. *J Med Genet* 2005;**42**:639–647.
28. Zwerger M, Roschitzki-Voser H, Zbinden R, Denais C, Herrmann H, Lammerding J, Grutter MG, Medalia O. Altering lamina assembly reveals lamina-dependent and -independent functions for A-type lamins. *J Cell Sci* 2015;**128**:3607–3620.
29. Bilińska ZT, Sylvius N, Grzybowski J, Fidziańska A, Michalak E, Walczak E, Walski M, Bieganowska K, Szymaniak E, Kuśmierczyk-Droszcz B, Lubiszewska B, Wagner T, Tesson F, Ruzyłło W. Dilated cardiomyopathy caused by LMNA mutations. Clinical and morphological studies. *Kardiol Pol* 2006;**64**:812–819. discussion 820-811.
30. Gupta P, Bilinska ZT, Sylvius N, Boudreau E, Veinot JP, Labib S, Bolongo PM, Hamza A, Jackson T, Ploski R, Walski M, Grzybowski J, Walczak E, Religa G, Fidzianska A, Tesson F. Genetic and ultrastructural studies in dilated cardiomyopathy patients: a large deletion in the lamin A/C gene is associated with cardiomyocyte nuclear envelope disruption. *Basic Res Cardiol* 2010;**105**:365–377.
31. Fidziańska A, Bilińska ZT, Tesson F, Wagner T, Walski M, Grzybowski J, Ruzyłło W, Hausmanowa-Petrusewicz I. Obliteration of cardiomyocyte nuclear architecture in a patient with LMNA gene mutation. *J Neurol Sci* 2008;**271**:91–96.
32. Fatkin D, MacRae C, Sasaki T, Wolff MR, Porcu M, Frenneaux M, Atherton J, Vidaillet HJ, Spudich S, De Girolami U, Seidman JG, Seidman C, Muntoni F, Müehle G, Johnson W, McDonough B. Missense mutations in the rod domain of the lamin A/C gene as causes of dilated cardiomyopathy and conduction-system disease. *N Engl J Med* 1999;**341**:1715–1724.
33. van Tintelen JP, Hofstra RM, Katerberg H, Rossenbacker T, Wiesfeld AC, Du Marchie Sarvaas GJ, Wilde AA, van Langen IM, Nannenberg EA, van der Kooi AJ, Kraak M, van Gelder IC, van Veldhuisen DJ, Vos Y, van den Berg MP. Working Group on Inherited Cardiac Disorders I, I.teruniversity Cardiology Institute of The Netherlands. High yield of LMNA mutations in patients with dilated cardiomyopathy and/or conduction disease referred to cardiogenetics outpatient clinics. *Am Heart J* 2007;**154**:1130–1139.
34. Bridger JM, Kill IR, O'Farrell M, Hutchison CJ. Internal lamin structures within G1 nuclei of human dermal fibroblasts. *J Cell Sci* 1993;**104 (pt. 2)**: 297–306.
35. Machiels BM, Broers JL, Raymond Y, de Ley L, Kuijpers HJ, Caberg NE, Ramaekers FC. Abnormal A-type lamin organization in a human lung carcinoma cell line. *Eur J Cell Biol* 1995;**67**:328–335.
36. Spann TP, Moir RD, Goldman AE, Stick R, Goldman RD. Disruption of nuclear lamin organization alters the distribution of replication factors and inhibits DNA synthesis. *J Cell Biol* 1997;**136**:1201–1212.
37. Jagatheesan G, Thanumalayan S, Muralikrishna B, Rangaraj N, Karande AA, Parnaik VK. Colocalization of intranuclear lamin foci with RNA splicing factors. *J Cell Sci* 1999;**112 (pt. 24)**: 4651–4661.
38. Buehler M, Keten S, Ackbarow T. Theoretical and computational hierarchical nanomechanics of protein materials: deformation and fracture. *Progress in Materials Science* 2008;**53**:1101–1241.
39. Kreplak L, Doucet J, Briki F. Unraveling double stranded alpha-helical coiled coils: an x-ray diffraction study on hard alpha-keratin fibers. *Biopolymers* 2001;**58**:526–533.
40. Bertaud J, Qin Z, Buehler MJ. Intermediate filament-deficient cells are mechanically softer at large deformation: a multi-scale simulation study. *Acta Biomater* 2010;**6**: 2457–2466.
41. Qin Z, Kreplak L, Buehler M. Nanomechanical properties of vimentin intermediate filament dimers. *Nanotechnology* 2009;**20**:425101.
42. Guzmán C, Jeney S, Kreplak L, Kasas S, Kulik AJ, Aebi U, Forró L. Exploring the mechanical properties of single vimentin intermediate filaments by atomic force microscopy. *J Mol Biol* 2006;**360**:623–630.
43. Fudge DS, Gardner KH, Forsyth VT, Riekel C, Gosline JM. The mechanical properties of hydrated intermediate filaments: insights from hagfish slime threads. *Biophys J* 2003; **85**:2015–2027.
44. Kreplak L, Doucet J, Dumas P, Briki F. New aspects of the alpha-helix to beta-sheet transition in stretched hard alpha-keratin fibers. *Biophys J* 2004;**87**:640–647.
45. Lanzicher T, Martinelli V, Long CS, Del Favero G, Puzzi L, Borelli M, Mestroni L, Taylor MR, Sbaizero O. AFM single-cell force spectroscopy links altered nuclear and cytoskeletal mechanics to defective cell adhesion in cardiac myocytes with a nuclear lamin mutation. *Nucleus* 2015;**6**:394–407.
46. Lanzicher T, Martinelli V, Puzzi L, Del Favero G, Codan B, Long CS, Mestroni L, Taylor MR, Sbaizero O. The cardiomyopathy lamin A/C D192G mutation disrupts

whole-cell biomechanics in cardiomyocytes as measured by atomic force microscopy loading-unloading curve analysis. *Sci Rep* 2015;**5**:13388.
47. Ramos FJ, Chen SC, Garelick MG, Dai DF, Liao CY, Schreiber KH, MacKay VL, An EH, Strong R, Ladiges WC, Rabinovitch PS, Kaeberlein M, Kennedy BK. Rapamycin reverses elevated mTORC1 signaling in lamin A/C-deficient mice, rescues cardiac and skeletal muscle function, and extends survival. *Sci Transl Med* 2012;**4**:144ra103.
48. Choi JC, Muchir A, Wu W, Iwata S, Homma S, Morrow JP, Worman HJ. Temsirolimus activates autophagy and ameliorates cardiomyopathy caused by lamin A/C gene mutation. *Sci Transl Med* 2012;**4**:144ra102.
49. Muchir A, Pavlidis P, Decostre V, Herron AJ, Arimura T, Bonne G, Worman HJ. Activation of MAPK pathways links LMNA mutations to cardiomyopathy in Emery-Dreifuss muscular dystrophy. *J Clin Invest* 2007;**117**:1282–1293.
50. Zhang W, Liu HT. MAPK signal pathways in the regulation of cell proliferation in mammalian cells. *Cell Res* 2002;**12**:9–18.
51. Communal C, Sumandea M, de Tombe P, Narula J, Solaro RJ, Hajjar RJ. Functional consequences of caspase activation in cardiac myocytes. *Proc Natl Acad Sci U S A* 2002;**99**:6252–6256.
52. Kumar A, Crawford K, Close L, Madison M, Lorenz J, Doetschman T, Pawlowski S, Duffy J, Neumann J, Robbins J, Boivin GP, O'Toole BA, Lessard JL. Rescue of cardiac alpha-actin-deficient mice by enteric smooth muscle gamma-actin. *Proc Natl Acad Sci U S A* 1997;**94**:4406–4411.
53. Zwerger M, Jaalouk DE, Lombardi ML, Isermann P, Mauermann M, Dialynas G, Herrmann H, Wallrath LL, Lammerding J. Myopathic lamin mutations impair nuclear stability in cells and tissue and disrupt nucleo-cytoskeletal coupling. *Hum Mol Genet* 2013;**22**:2335–2349.
54. Dahl KN, Scaffidi P, Islam MF, Yodh AG, Wilson KL, Misteli T. Distinct structural and mechanical properties of the nuclear lamina in Hutchinson-Gilford progeria syndrome. *Proc Natl Acad Sci U S A* 2006;**103**:10271–10276.
55. Verstraeten VL, Ji JY, Cummings KS, Lee RT, Lammerding J. Increased mechanosensitivity and nuclear stiffness in Hutchinson-Gilford progeria cells: effects of farnesyltransferase inhibitors. *Aging Cell* 2008;**7**:383–393.
56. Caille N, Thoumine O, Tardy Y, Meister JJ. Contribution of the nucleus to the mechanical properties of endothelial cells. *J Biomech* 2002;**35**:177–187.
57. Guilak F, Mow VC. The mechanical environment of the chondrocyte: a biphasic finite element model of cell-matrix interactions in articular cartilage. *J Biomech* 2000;**33**:1663–1673.
58. Rowat AC, Jaalouk DE, Zwerger M, Ung WL, Eydelnant IA, Olins DE, Olins AL, Herrmann H, Weitz DA, Lammerding J. Nuclear envelope composition determines the ability of neutrophil-type cells to passage through micron-scale constrictions. *J Biol Chem* 2013;**288**:8610–8618.
59. Versaevel M, Riaz M, Grevesse T, Gabriele S. Cell confinement: putting the squeeze on the nucleus. *Soft Matter* 2013;**9**:6665–6676.
60. Rowat AC, Foster LJ, Nielsen MM, Weiss M, Ipsen JH. Characterization of the elastic properties of the nuclear envelope. *J R Soc Interface* 2005;**2**:63–69.
61. Dorner D, Gotzmann J, Foisner R. Nucleoplasmic lamins and their interaction partners, LAP2alpha, Rb, and BAF, in transcriptional regulation. *FEBS J* 2007;**274**:1362–1373.
62. Kolb T, Maaß K, Hergt M, Aebi U, Herrmann H. Lamin A and lamin C form homodimers and coexist in higher complex forms both in the nucleoplasmic fraction and in the lamina of cultured human cells. *Nucleus* 2011;**2**:425–433.
63. Mounkes LC, Kozlov SV, Rottman JN, Stewart CL. Expression of an LMNA-N195K variant of A-type lamins results in cardiac conduction defects and death in mice. *Hum Mol Genet* 2005;**14**:2167–2180.
64. Bechert K, Lagos-Quintana M, Harborth J, Weber K, Osborn M. Effects of expressing lamin A mutant protein causing Emery-Dreifuss muscular dystrophy and familial partial lipodystrophy in HeLa cells. *Exp Cell Res* 2003;**286**:75–86.
65. Scharner J, Gnocchi VF, Ellis JA, Zammit PS. Genotype-phenotype correlations in laminopathies: how does fate translate? *Biochem Soc Trans* 2010;**38**:257–262.
66. Barascu A, Le Chalony C, Pennarun G, Genet D, Imam N, Lopez B, Bertrand P. Oxidative stress induces an ATM-independent senescence pathway through p38 MAPK-mediated lamin B1 accumulation. *EMBO J* 2012;**31**:1080–1094.
67. Wu W, Muchir A, Shan J, Bonne G, Worman HJ. Mitogen-activated protein kinase inhibitors improve heart function and prevent fibrosis in cardiomyopathy caused by mutation in lamin A/C gene. *Circulation* 2011;**123**:53–61.